Earthquake Scenario Ground Motions for the Urban Area of Evansville, Indiana

Jennifer S. Haase and Robert L. Nowack
Purdue University

INTRODUCTION

The Wabash Valley seismic zone and the New Madrid seismic zone are the closest large earthquake source zones to Evansville, Indiana. The New Madrid earthquakes of 1811–1812, more than 180 km from Evansville, produced ground motions with Modified Mercalli Intensity VII near Evansville. Liquefaction evidence has been documented less than 40 km away from Evansville resulting from two large earthquakes that occurred within the past 12,000 years in the Wabash Valley. Two earthquake scenarios are described in this paper that demonstrate the expected ground motions within the 33 by 42 km^2 region around Evansville based on a repeat earthquake from each of these source regions. The simulations take into account the 1-D amplification of ground motion in the unconsolidated soil layer using a new laterally varying model of seismic velocity and bedrock depth. The objective of this work is to demonstrate to what extent the local variability in ground motions due to local site effects impacts the assessment of seismic hazard. These scenario maps are a valuable complement to the probabilistic seismic hazard maps for the same area (Haase, Nowack, Choi, and Bowling 2011) because the scenario maps illustrate the direct relationship between an earthquake source and the potential hazard. Also, the scenario ground motions can be used to calculate liquefaction hazard (Haase, Nowack, and Choi 2011). These ground motion maps, along with those for the probabilistic seismic hazard and liquefaction hazard, will be useful for evaluating the potential losses from earthquakes and can be used for planning, development, hazard mitigation, and emergency response.

Two earthquake source zones near Evansville, Indiana, that are considered capable of producing an **M** 6.5 or greater earthquake are the New Madrid seismic zone, near New Madrid, Missouri, and the Wabash Valley seismic zone along the southern border between Illinois and Indiana. The New Madrid fault ruptured in a series of three great earthquakes in 1811–1812, which were felt over a large area in the central and eastern United States (Hough *et al.* 2000; Nuttli 1983). Several estimates of magnitude for the three events have been made: **M** 7.2, **M** 7.0, **M** 7.5 (Hough *et al.* 2000), **M** 7.6, **M** 7.5, **M** 7.8 (Bakun and Hopper 2004), **M** 8.1, **M** 7.8, **M** 8.0 (Johnston 1996). The Evansville area experienced a Modified Mercalli Intensity VII from these events, the highest intensity observed in Indiana (Stover and Coffman 1993). Eight earthquakes of magnitude greater than about 6 have occurred in southern Illinois and Indiana, based on paleoliquefaction evidence found in river banks throughout those states (Munson and Munson 1996; Wheeler and Cramer 2002). The largest two have occurred in the Wabash Valley seismic zone and have estimated magnitudes of **M** 7.5 for the Vincennes earthquake at approximately 6,100 before present (BP) (Green *et al.* 2005) and **M** 6.7 for the Skelton–Mt. Carmel earthquake at approximately 12,000 BP (Olson *et al.* 2005). Both of these events produced liquefaction features in the Wabash Valley at distances comparable to the distance to Evansville, although there have been no features discovered within the study region. The two earthquake scenarios chosen for this study are based on a possible recurrence of a New Madrid earthquake of **M** 7.7 and a Skelton–Mt. Carmel type earthquake of **M** 6.8 in the Wabash Valley. While future earthquakes may not occur on exactly the same fault or with the same size and mechanism as past earthquakes, these scenarios are useful for illustrating the amplification effects of near surface geology for events from these source areas. Note that all magnitudes in this paper are moment magnitude.

We consider a strong-to-major earthquake to be a much more likely event in New Madrid than in the Wabash Valley. A recurrence interval of approximately 500 years has been estimated from radiometric and archaeological dating of liquefaction features from large earthquakes occurring in the New Madrid seismic zone (Tuttle *et al.* 2005, 2002). However, low rates of deformation observed by GPS in the midcontinent indicate that present-day recurrence rates may be lower or that the deformation is not steady in time (Calais and Stein 2009). Currently a recurrence interval of 500 to 1,000 years for a strong-to-major event has been retained for the estimation of probabilistic seismic hazard in the 2008 U.S. Geological Survey National Seismic Hazard Maps (Frankel *et al.* 1996, 2002; Petersen *et al.* 2008). The Wabash Valley, on the other hand, has produced only four earthquakes greater than **M** 6 in 14,000 years (Green *et al.* 2005; McNulty and Obermeier 1999; Munson and Munson 1996; Munson *et al.* 1995; Olson *et al.* 2005; Pond 1996) which implies a significantly longer recurrence interval. While the characteristic earthquake model with time or slip predictable behavior may not be the best representation for mid-continent source zones, the large difference in probability of occurrence between the two source zones is reflected in the probabilistic seismic hazard estimates for the

doi: 10.1785/gssrl.82.2.177

area (Haase, Nowack, Choi, and Bowling 2011; Petersen *et al.* 2008). Assuming a Gutenberg-Richter relation for **M** 6 earthquakes in the greater Wabash Valley of approximately 0.002 per year (Wheeler and Cramer 2002), this would imply a rate on the order of 7×10^{-6} per year for a reduced area within 15 km of the prehistoric earthquake that occurred closest to Evansville, the Skelton–Mt. Carmel event. Deaggregation of the USGS National Seismic Hazard Maps (Harmsen *et al.* 1999) for ground motions with 2% probability of being exceeded in 50 years show that more than 25% of the contribution to the seismic hazard in Evansville comes from a New Madrid type earthquake of **M** 7 or greater, and less than 10% of the hazard comes from large magnitude (>**M** 6.8) Wabash Valley type events. It is useful to provide estimates of the hazard to Evansville from the Wabash Valley seismic zone, since the city is within this zone where strong to major earthquakes occurred throughout the Holocene and back into the Pleistocene. Extensive observations of prehistoric liquefaction features from these events have been made (Munson and Munson 1996), and moderate earthquakes have been recorded during historic times.

SCENARIO DEFINITION

The New Madrid scenario is defined by three hypothetical faults that follow the current earthquake activity near the locations of the 1811–1812 New Madrid earthquakes, although the greatest contribution comes from the closest (northern) segment. The Wabash Valley scenario event is set in a region of diffuse seismicity and follows the trend of Paleozoic geologic structures in the Wabash Valley near the location of the Skelton–Mt. Carmel earthquake.. The Wabash Valley scenario fault length estimate is assigned based on the corresponding magnitude (Wells and Coppersmith 1994). As there are no data to constrain the endpoints of this fault, it should be considered an illustration of one of many possible scenarios. Similarly, no attempt has been made to consider source directivity or variations in radiation pattern, depth, or stress drop. Because directivity of the source is not included, which would otherwise potentially allow constructive interference to increase ground motion levels, the greatest ground motions are generated by the closest fault segment for each scenario. The scenario faults are shown in Figure 1 and described in Table 1.

INPUT MODEL

The ground motion level at a given site may be amplified or deamplified depending on the local site geology. The input model used to calculate amplification describes the geologic material, bedrock depth, and seismic velocity at each point on a 0.01° × 0.01° grid for the nine-quadrangle region surrounding Evansville. At this scale, the maps presented here cannot be used in a site-specific manner, but rather as a guide to where more detailed studies are needed. The surficial geology (Gray 1989; Moore *et al.* 2009) along the Ohio River Valley near Evansville consists primarily of fluvial and lake deposits that fill incised valleys into Pennsylvanian-age bedrock (Figure 2). Wind-deposited loess covers the low surrounding hills. Beneath the terraces bordering the current river valley are alternating layers of outwash, slackwater lake deposits, and fluvial deposits. The geologic maps, in conjunction with subsurface information, are used to associate regions of similar depositional history and similar properties to representative shear wave velocity profiles.

A bedrock depth model has been produced based on water well logs (Bleuer 2000), depth measurements interpreted from *P*-wave refraction profiles (Rudman *et al.* 1973; Whaley *et al.* 2002), and bedrock elevation points from oil, gas, and water well logs. The model is described in detail in Haase *et al.* (2011). The points are interpolated for a smooth soil thickness model in the uplands area, where eolian deposition of loess dominates, and interpolated for a smooth bedrock elevation model in the lowland areas. These are combined with modifications made by hand to incorporate the steep contoured edges of the central bedrock valley based on individual high-quality well logs. The depth uncertainties are approximately 1.2 m in the uplands and 3.7 m in the lowlands. The perspective view shown in Figure 3 gives a good representation of the horizontal variability of the individual point measurements and illustrates the difference in model surface complexity imposed for the uplands and lowlands.

Cone penetrometer data with *S*-wave measurements (S-CPT) (Holzer 2003) and borehole shear wave velocity measurements (Eggert *et al.* 1994) are the primary source of data for determining the depth dependent shear wave velocities and are described in detail by Haase *et al.* (2011). These data are separated into four groups based on similarity in geotechnical properties within the soil column and the surficial geology. What we refer to as the river alluvium group includes floodplain deposits in the lowlands; the outwash terrace group includes terrace deposits at the edges of the Ohio River; the lacustrine group includes slackwater deposits of the lacustrine terraces; and the loess group includes eolian deposits over bedrock uplands. As shown by Haase *et al.* (2011), the velocity variations are not large, with velocities in the 150 to 250 m/s range for all groups, and with uncertainties on the order of 60 m/s. Figure 4 shows the assignment of the reference velocity profile information to the spatial grid points of the model.

METHOD

The calculation of the ground motion level at each point in the map area is based on the magnitude of the earthquake, the closest distance from the point to the fault, and the amplification factor at the local site. Attenuation relations estimate the ground motion level at different frequencies as a function of distance from and magnitude of the source. Because of the few instrumental recordings from moderate events, and the lack of instrumental recordings from large events in the central and eastern United States (CEUS) there is significant uncertainty in the predicted ground motions, especially for large magnitudes. For that reason, we use a weighted average of estimates from a suite of ground motion attenuation relationships (Table 2). These are the same ground motion attenuation relationships and respective weights that are used in the probabilistic hazard

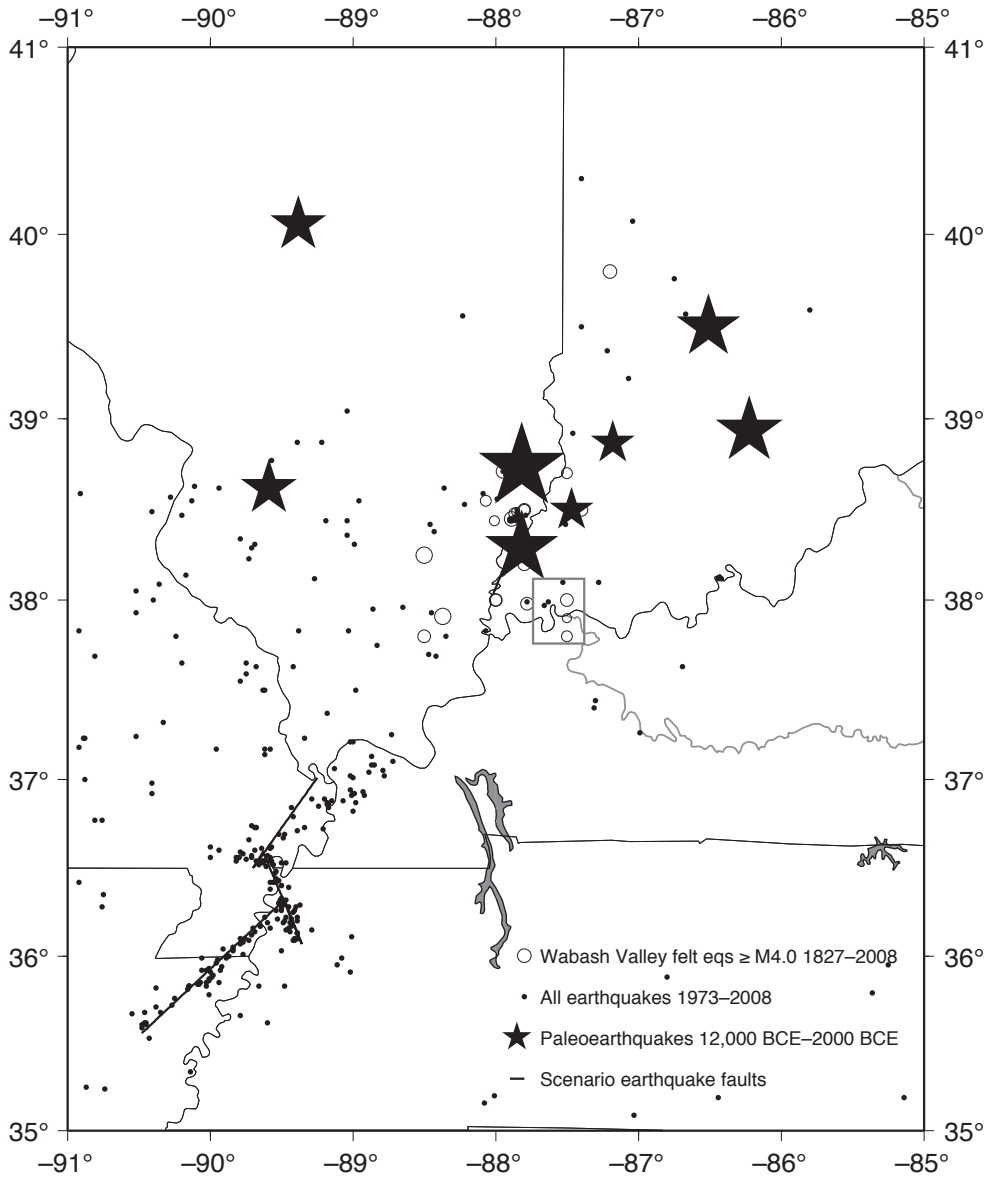

▲ **Figure 1.** Location of scenario earthquake faults in the Wabash Valley and New Madrid (black lines) relative to historical earthquakes (Seeber and Armbruster 1991), current earthquakes (Sipkin *et al.* 2000), and earthquake energy centers from large prehistoric earthquakes in the southern Illinois basin from 12,000 to 2000 B.C.E. (Wheeler and Cramer 2002). The Evansville study area is indicated by the small rectangle.

TABLE 1
Source Parameters for Scenario Earthquakes

Source Zone	Magnitude	Distance to Evansville	Fault Coordinates
Wabash Valley	6.8	40 km	38.29 –87.89
			38.03 –88.02
New Madrid	7.7	180 km	35.56 –90.48
			36.32 –89.48
			36.07 –89.36
			36.59 –89.63
			36.50 –89.70
			37.01 –89.25

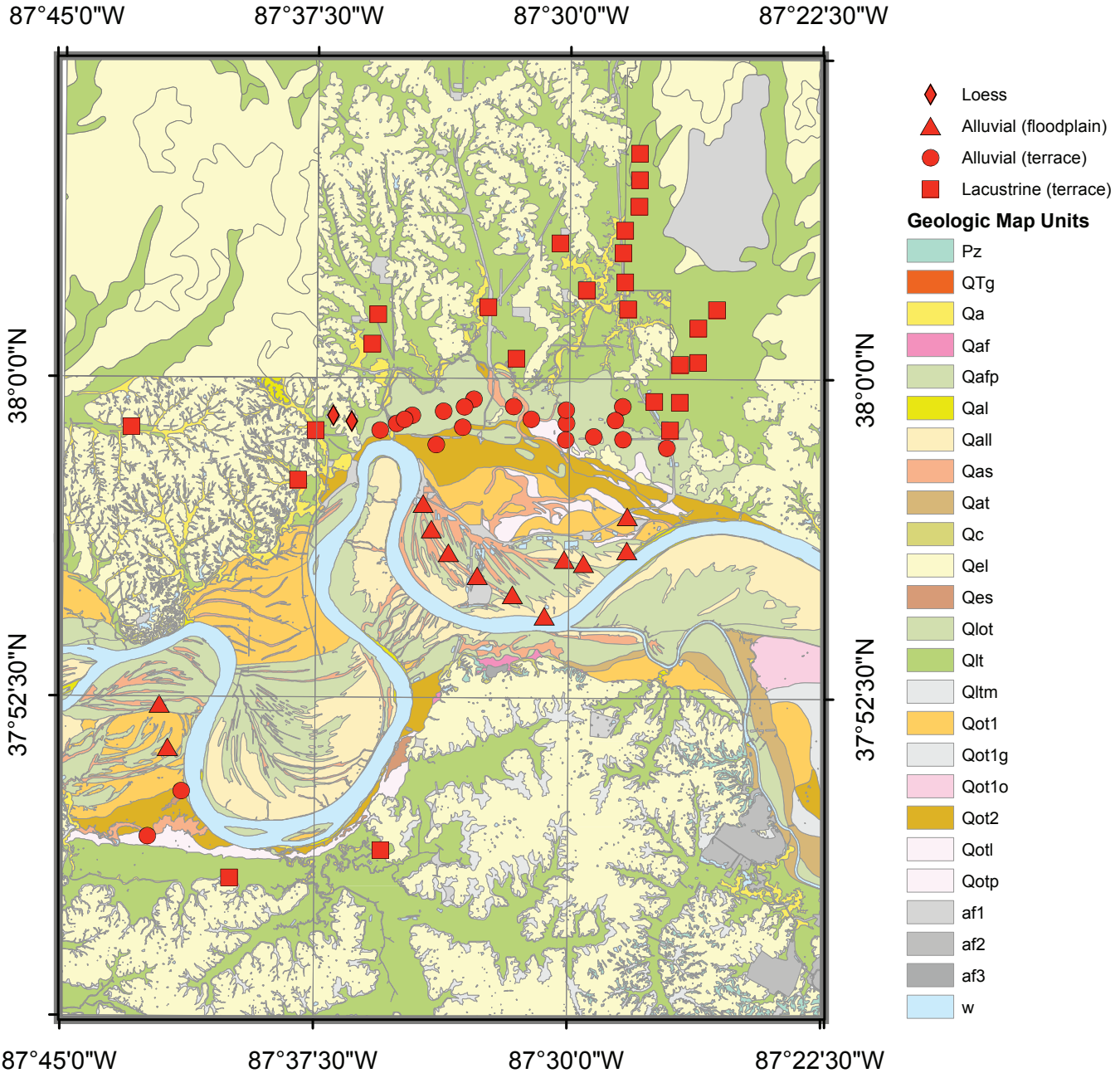

▲ **Figure 2.** Surficial geologic map (Moore *et al.* 2009). Mapped units are Qc—Colluvium, Qal—Alluvium, Qall— Levee deposit alluvium, Qas—Alluvium in modern floodplain sloughs, Qaf—alluvium in alluvial fans, Qafp—River floodplain alluvium, Qat—Low terrace alluvium, Qa—Creek and sheetwash alluvium, Qes—Dune sand, Qel—Loess, Qot1o—Reworked Ohio River terrace outwash alluvium, Qot1g—Reworked Green River terrace alluvium, Qltm—Upland marginal lacustrine deposits, Qlt—Lacustrine terrace slackwater deposits, Qot1—Low terrace outwash alluvium, Qlot—Lacustrine and outwash terrace deposits, Qotp—Paleolevee deposits on outwash terrace, Qot2—High terrace outwash alluvium, QTg—Upland gravel, Pz—Paleozoic bedrock, w—Surface water, af1, af2, af3—Artificial fill. Cone penetometer test locations where shear wave velocities were measured are shown as red symbols. Loess symbols indicate borehole shear wave measurement locations.

calculation for the Evansville area (Haase, Nowack, Choi, and Bowling 2011) and for the USGS National Seismic Hazard Maps (Petersen *et al.* 2008).

The amplification factor is calculated using a frequency domain approach assuming shear waves vertically incident on a localized 1-D bedrock/soil profile (SHAKE91; Idriss and Sun 1992). It takes into account nonlinear behavior of the soil column using an iterative equivalent linear approach. The uncertainties in the bedrock depth and shear wave velocities at each point were calculated from the distribution of available data during the construction of the input model. Random variations from this distribution are introduced in the bedrock depth and

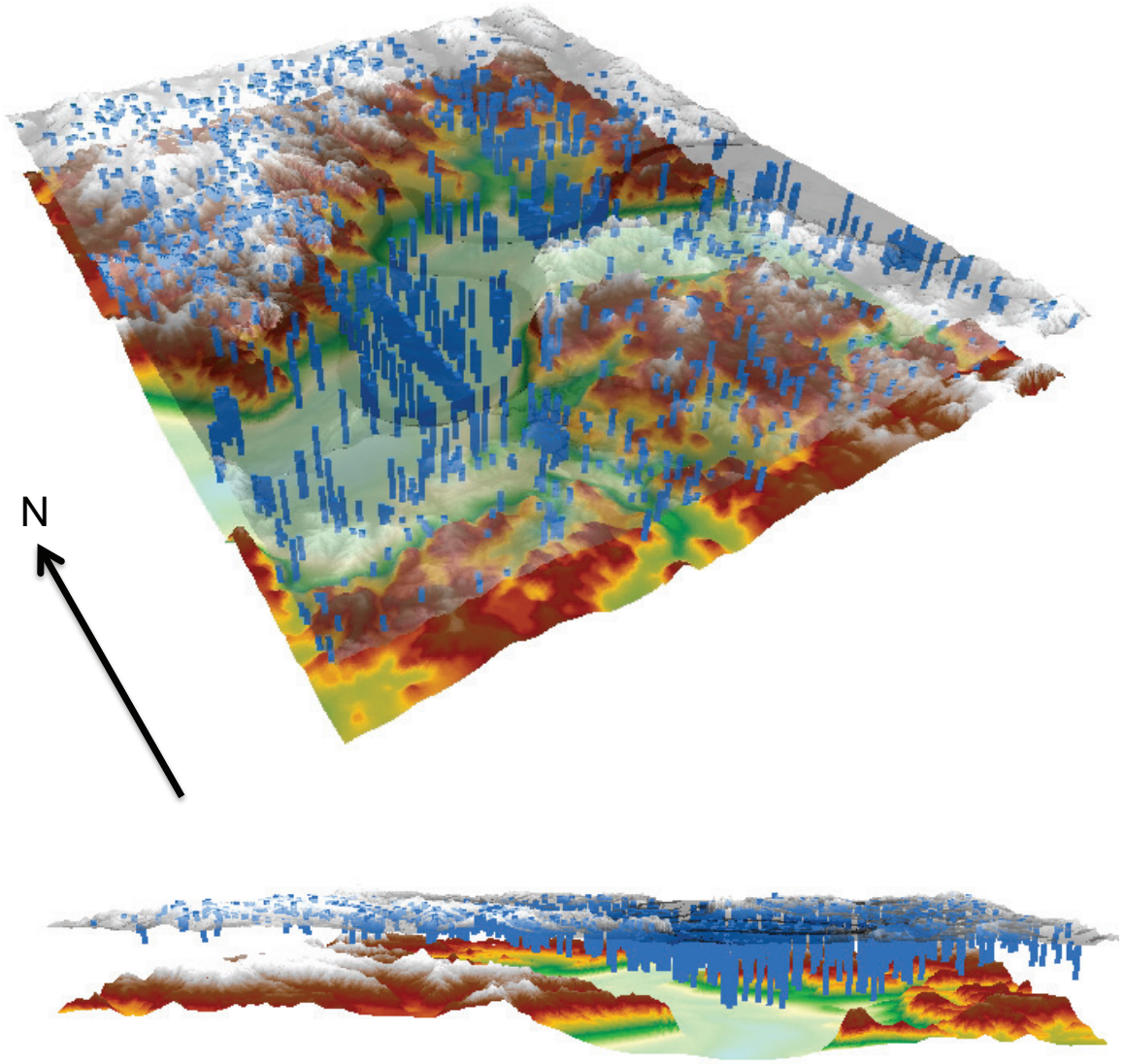

▲ **Figure 3.** Top: Perspective views of the surface digital elevation model (DEM) (shown as the upper gray transparent surface with 20× vertical exaggeration), and derived bedrock elevation (shown as the lower surface in color with 35× exaggeration). The offset between the two surfaces is exaggerated to increase the visibility. Individual bedrock depth measurements are illustrated with blue bars with 20× exaggeration. Bottom: Side view from the west of the surface and bedrock elevation. Note the difference in density of the uplands point measurements and the lowlands point measurements, and the horizontal variability in their depth. Maximum depth from the surface to bedrock is 55 m.

velocity profile at each point to calculate the corresponding distribution of amplification factors. One hundred realizations of the random profiles are used. Random variations from the average modulus reduction curves and damping curves are also introduced to account for uncertainty in the knowledge of the true nonlinear behavior. To account for uncertainty in the response due to the uncertainty in the input bedrock ground motion at the soil/bedrock interface, we select randomly from a set of 16 ground motion time series for each realization. The randomized soil profiles and scaled ground motions are then used as input to the site response calculation to create a distribution of possible site-amplification factors at each site for varying levels of input bedrock ground motion.

TABLE 2
Attenuation Relationships Used in the Scenario Ground Motion Calculations

Attenuation Curve Reference	Weight
Toro *et al.* (1997)	0.2
Frankel *et al.* (1996)	0.1
Campbell and Bozorgnia (2003)	0.1
Atkinson and Boore (2006)—140 bar stress drop	0.1
Atkinson and Boore (2006)—200 bar stress drop	0.1
Tavakoli and Pezeshk (2005)	0.1
Silva *et al.* (2002)	0.1
Somerville *et al.* (2001)	0.2

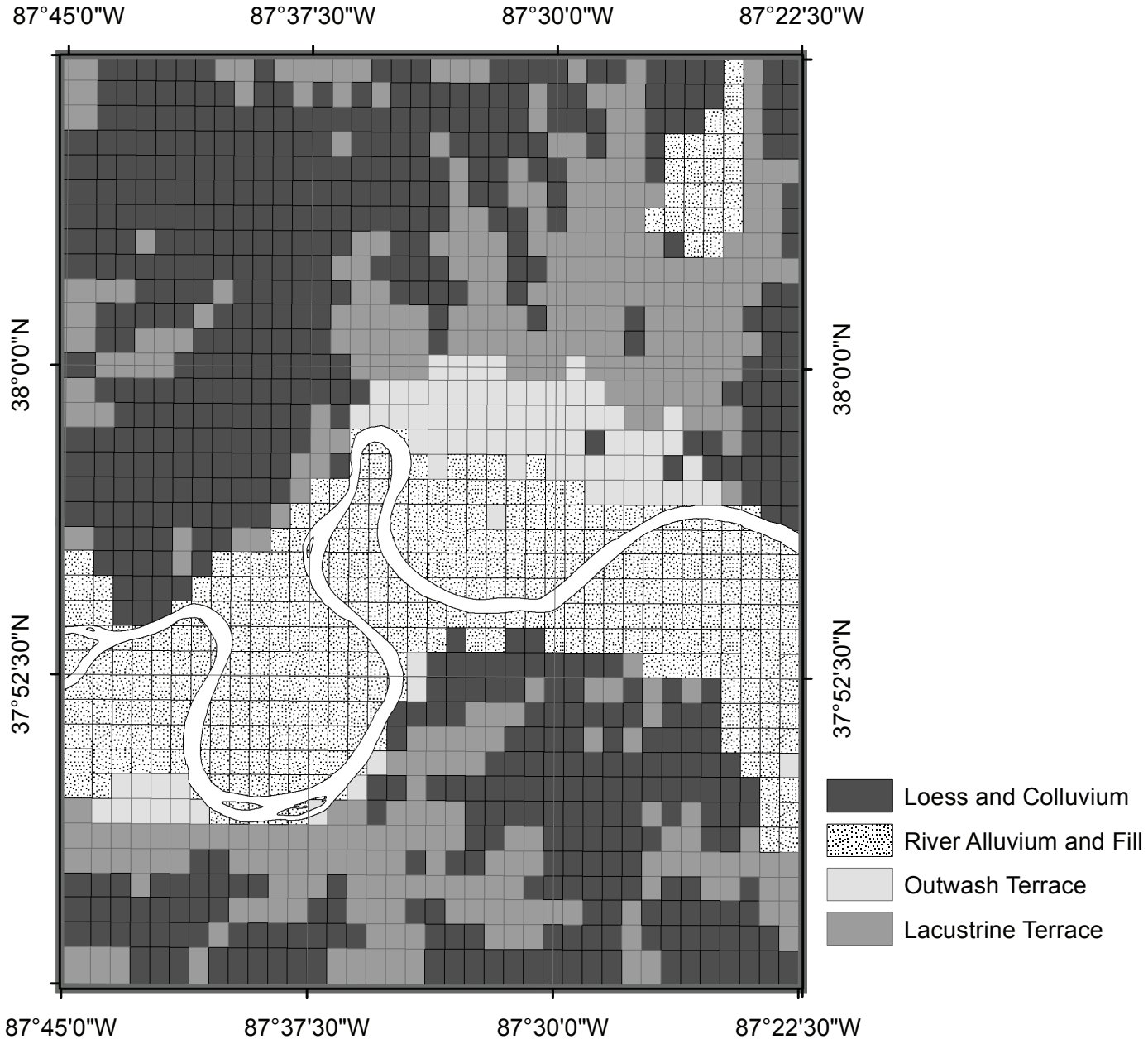

▲ **Figure 4.** Assignment of velocity profile characteristics at 0.01° × 0.01° grid cell size based on the geologic unit with the predominant surface area within the cell.

It is necessary to estimate the amplification at different input bedrock ground motion levels, because the behavior of the material changes at high strain (Idriss and Sun 1992). Therefore, the resulting amplification factor could be different and even smaller for greater input ground motion levels. The capability to model this nonlinear behavior is important, as it has important consequences for the final hazard map. Cramer (2006) discusses the validation, particularly at strong levels of input ground motion, of the modified version of SHAKE91 used in this application, with other equivalent linear and nonlinear codes.

The resulting amplification factors are tabulated at 20 different input ground motion levels and seven different response periods (pga, 0.1 s, 0.2 s, 0.3 s, 0.5 s, 1.0 s, and 2.0 s). The uncertainty is also calculated, based on the 100 realizations that were carried out for each tabulated value. The subsurface model and resulting amplification factors are the same as those used in the probabilistic seismic hazard calculation, and are described in detail in Haase *et al.* (2011).

In the final step, the median site amplification is interpolated from the tabulated values for the appropriate median hard-rock ground motion given by the attenuation relations. The amplification factor multiplies the ground motion from each of the eight attenuation relations, then the weighted average of the eight estimates is calculated to determine the final value of acceleration at the grid point. The resulting sce-

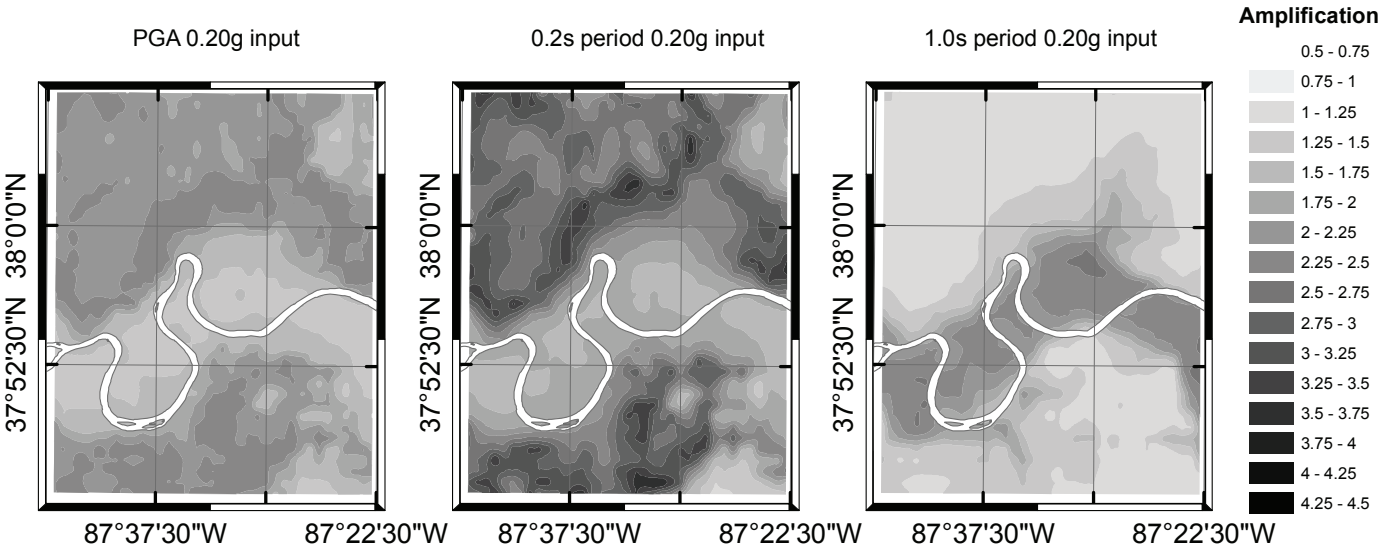

▲ **Figure 5.** (left) Amplification factors for PGA, (center) 0.2 s spectral acceleration, and (right) 1.0 s spectral acceleration, all calculated with 0.2 g input bedrock ground motions.

nario maps represent the median ground motion expected for the given scenario earthquake, which are the ground motions one expects will be exceeded 50 percent of the time when that scenario earthquake occurs. This calculation is implemented using the program hazFXnga7c.f (provided by Mark Petersen, USGS) in the deterministic mode, which has been modified to multiply the hard-rock ground motion from each attenuation relation by that site's hard-rock amplitude-dependent site amplification using the above described procedure, similar to the approach of Cramer *et al.* (2004) for Memphis, Tennessee.

Figure 5 shows the amplification factors for an input bedrock ground motion level of 0.2 g for pga, 0.2 s period, and 1.0 s period. At 0.2 s, which is the period that most affects shorter structures, the amplification is due to resonances in unconsolidated soils between 10 and 15 meters thick. This appears as high amplification near the borders between the uplands and river terraces on both sides of the Ohio River. A recent study of the 2008 $M = 5.4$ Mt. Carmel earthquake in Illinois showed site resonances in this range for USIN and EVIN, two seismic stations found within the study area (Odum *et al.* 2010). On the other hand, at 1.0 s period, the higher amplifications are in the thickest soils within the ancient bedrock valley and extending to the north under the terrace alluvium deposits beneath Evansville. The range of amplification factors is comparable to that assigned to NEHRP site class B to class D for 1.0 s periods. For 0.2 s period, however, the range of amplification factors calculated here is much greater than that typically assigned to NEHRP site class B to class D.

The 1-D calculation may not fully capture the 3-D response near the edges of the steep-sided bedrock valley. The general results of Bard and Bouchon (1985) that describe 2-D response of sediment-filled valleys as a function of the valley aspect ratio and the velocity contrast of materials at the base of the basin would suggest that a basin of this size would have a response close to 1-D at the center of the valley. However, future work should investigate the effects at the valley edges using 3-D calculations. The uncertainties associated with the bedrock depth and soil velocity models, as well as the approximations made in the calculation of the response, should be kept in mind when using the amplification maps, as they cannot be considered site specific.

SCENARIO SEISMIC HAZARD RESULTS

The scenario seismic hazard maps have been computed for peak ground acceleration (PGA) and spectral accelerations at 0.1, 0.2, 0.3, 0.5, 1.0, and 2.0 s for a New Madrid magnitude 7.7 scenario event and for a Wabash Valley 6.8 scenario event. The PGA, 0.2 s, and 1.0 s maps are shown in Figure 6 .

For the New Madrid scenario PGA, the highest accelerations of 0.15 g to 0.2 g are in the southern part of the study area, which is consistent with the fact that the New Madrid fault is to the southwest of Evansville, but the ground motion levels increase again on the farther side of the river due to local site conditions. Table 3 illustrates the range of potential damage corresponding to these ground motion levels, an approximation that can be improved by using estimates of peak ground velocity at higher intensities (Wald *et al.* 1999). At 0.2 s spectral acceleration, the highest values of 0.4 g to 0.5 g are again seen away from the bedrock valley and correspond to thinner soils and therefore shorter periods. It is impressive to note that the accelerations at such high frequencies are significant despite the fact that the source is 180 km away, and this re-emphasizes the low attenuation of seismic waves in the center of North America. Fortunately, the highest ground motions at this period occur southwest of the major urban areas in Evansville and Henderson, Kentucky. The highest 1.0 s spectral accelerations are 0.15 to 0.17 g and occur where the soil is thickest, associated with the ancient bedrock valley. This region of higher ground motion (up to 0.17 g) extends into the terrace deposits on which most of Evansville is built. It also extends significantly east from the river under Henderson.

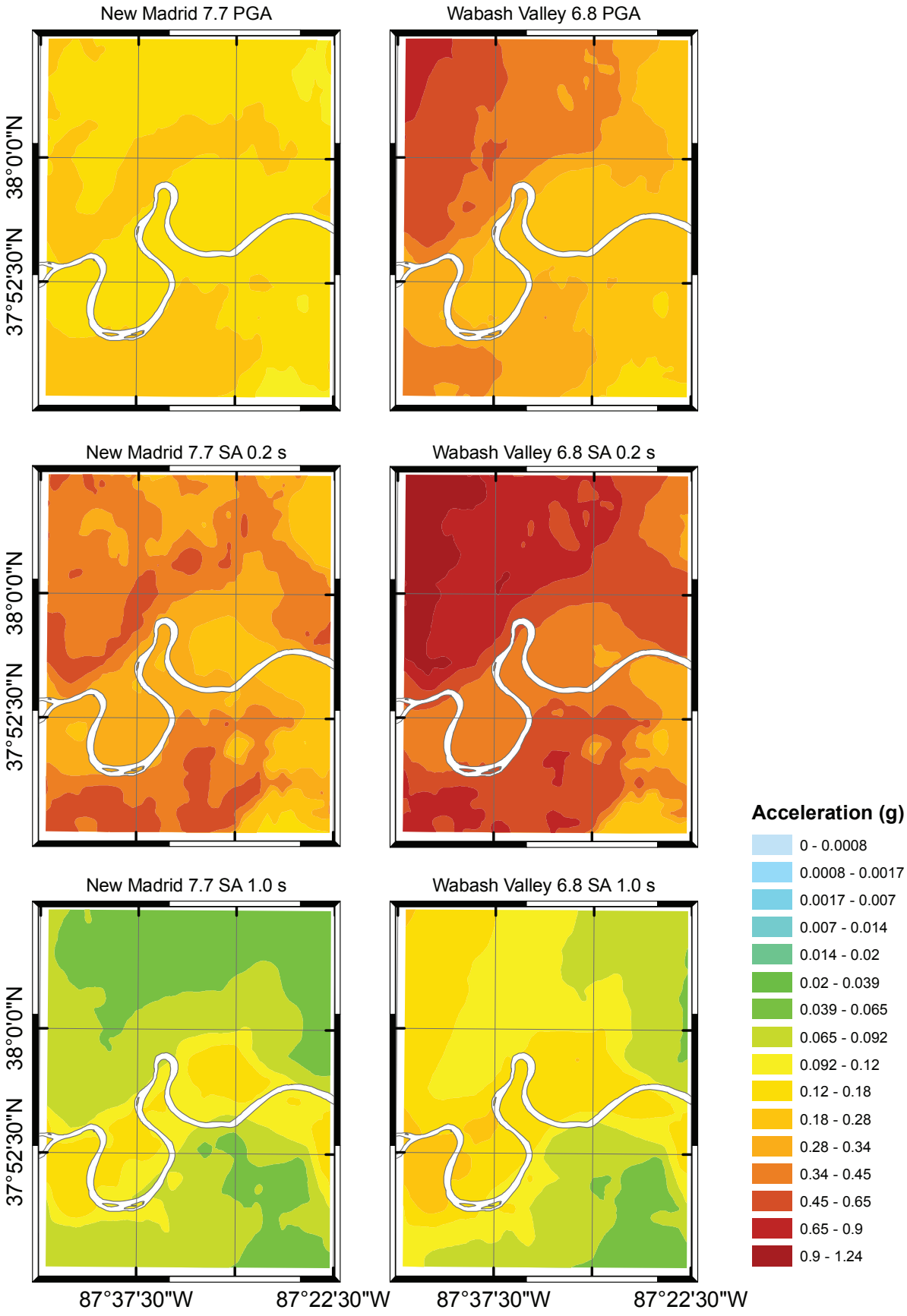

▲ **Figure 6.** Ground motions for (left column) an **M** 7.7 New Madrid scenario event and (right column) an **M** 6.8 Wabash Valley scenario event. From top to bottom, the figures show PGA, 0.2 s spectral acceleration, and 1.0 s spectral acceleration.

TABLE 3
Relation between acceleration and intensity of felt effects (Wald et al., 1999).

Perceived Shaking	Potential Damage	Peak Acc (g)	Instrumental Intensity
Not felt	None	< 0.0017	I
Weak	None	0.0017–0.014	II–III
Light	None	0.014–0.039	IV
Moderate	Very light	0.039–0.092	V
Strong	Light	0.092–0.18	VI
Very strong	Moderate	0.18–0.34	VII
Severe	Moderate/Heavy	0.34–0.65	VIII
Violent	Heavy	0.65–1.24	IX
Extreme	Very Heavy	>1.24	IX+

For the Wabash Valley scenario, the highest PGAs are 0.6 to 0.8 g in the northwest corner of the map area with accelerations decreasing toward the southeast. PGA values in Evansville are in the 0.2 to 0.4 g range. The decrease in acceleration toward the southeast corner is a direct result of the distance to the seismic source. For 0.2 s spectral acceleration, the values exceed 1.0 g in the northwest corner and decrease to levels of about 0.3 g in the central Evansville urban area north of the Ohio River. The 0.2 s spectral acceleration increases again south of the river with values of 0.4 to 0.7 g. At 1.0 s spectral acceleration the pattern of amplified ground motion above the bedrock valley is superimposed on the distance-dependent decrease in ground motion level. The 1.0 spectral acceleration is 0.2 to 0.25 g in soil deposits underlying the Ohio River floodplain and terraces.

CONCLUSIONS

Ground motions from an **M** 6.8 Wabash Valley scenario earthquake centered 40 km northwest of the city, similar to what may have occurred during the Skelton–Mt. Carmel earthquake about 12,000 years ago, would be very strong across the Evansville area. Peak ground acceleration would vary from 0.8 g in the region northwest of Evansville to 0.1 g in the southeast as distance increases from the causative fault. Local soil conditions have a major impact on the ground motions predicted for the scenario earthquakes. Ground motions decrease with distance from 1.5 g to 0.3 g for 0.2 s spectral acceleration when they reach the main part of Evansville, but then increase again in amplitude from 0.3 to 0.6 g south of the city and the Ohio River. Accelerations south of the river 15 km further away from the earthquake source are comparable to those just north of the river. The majority of the urban area is constructed on alluvial and lacustrine terrace deposits north of the Ohio River, over an ancient incised bedrock valley. The thickness of the deposits within that bedrock valley is such that resonances produce strong amplification at 1.0 s period. The resulting ground motions at 1.0 s spectral accelerations are 0.1 to 0.25 g in the Ohio River Valley.

The peak ground acceleration level for a magnitude 7.7 New Madrid scenario event, similar to what may have occurred during the 1811–1812 New Madrid earthquakes, would be about 0.15 to 0.25 g, with significant local variations across the study area. The 0.2 s spectral accelerations would be very high, between 0.4 and 0.5 g, north and west of the main urban center of Evansville on the north side of the river. The 1.0-s spectral accelerations would be 0.05 to 0.16 g, with higher values confined to the bedrock valley. Variations in the level of acceleration caused by local variations in site conditions are greater than the distance-dependent variations of ground motion across the study area due to the attenuation relations. The densest urbanization in Evansville on the north side of the river and Henderson, Kentucky, on the south side of the river, is within the area of preferential amplification at 1.0 s period for both scenarios, but these areas experience relatively less amplification than surrounding areas at 0.2 s. This is consistent with expected resonance periods based on the soil profiles and bedrock depth.

The objective of this work is to demonstrate the local variability in ground motions due to only one factor in the ground motion equation—local site effects. This study does not attempt to examine complexity in the source or 3-D wave propagation that may also cause variability in the ground motions. These factors would be most significant for the closer Wabash Valley event. We expect that the more distant New Madrid source would be more likely to produce a more nearly homogeneous wavefield impinging on the study area, so that the pattern of variations calculated here would be a realistic representation of ground motion variability.

These scenario maps are a valuable complement to the probabilistic seismic hazard maps for the same area (Haase, Nowack, Choi, and Bowling 2011), because the scenario maps illustrate the direct relationship between an earthquake source and the potential hazard. Also, the scenario ground motions can be used to calculate liquefaction hazard (Haase, Nowack, and Choi 2011). However, scenario ground motions do not communicate effectively the relative probability of occurrence of these events, which may be as infrequent as one in 4,000 years for the Wabash Valley event, *i.e.*, very rare, to one in 500–1,000 years for the New Madrid event. The scenario maps are most effective in combination with the probabilistic seismic hazard maps, which indicate the probability that a given ground motion level will be exceeded in a specified amount of time.

ACKNOWLEDGMENTS

This work was supported by the USGS National Earthquake Hazards Reduction Program (grant G09AP00057). Chris Cramer and Mark Petersen provided software for the scenario ground motion calculations. We sincerely thank Oliver Boyd, Chris Cramer, and Robert Bauer for their detailed reviews of this work. We would like to thank the members of the Evansville Area Earthquake Hazards Mapping Project Technical Working Group for their invaluable efforts in geological mapping and data collection and for their input into the decisions for the choice of scenario earthquakes. Key motivation for this project came from the Southwest Indiana Disaster Resistant Community Corporation. We appreciate the comprehensive reviews provided by Francesco Mulargia, Steve Harmsen, and Charles Mueller on an early version of this work. We thank Tim Bowling for assistance with the graphics.

REFERENCES

Atkinson, G., and D. M. Boore (2006). Earthquake ground-motion prediction equations for eastern North America. *Bulletin of the Seismological Society of America* **96** (6), 2,181–2,205.

Bakun, W. H., and M. G. Hopper (2004). Magnitudes and locations of the 1811–1212 New Madrid, Missouri, and the 1886 Charleston, South Carolina, earthquakes. *Bulletin of the Seismological Society of America* **94** (1), 64–75.

Bard, P. Y., and M. Bouchon (1985). The two-dimensional resonance of sediment-filled valleys. *Bulletin of the Seismological Society of America* **75** (2), 519–541.

Bleuer, N. K. (2000). *iLITH Database of the Indiana Geological Survey*. Open File Study 00-8 on CD-ROM. Bloomington: Indiana Geological Survey.

Calais, E., and S. Stein (2009). Time-variable deformation in the New Madrid seismic zone. *Science* **323** (5920), 1,442–1,442.

Campbell, K. W., and Y. Bozorgnia (2003). Updated near-source ground-motion (attenuation) relations for the horizontal and vertical components of peak ground acceleration and acceleration response spectra. *Bulletin of the Seismological Society of America* **93** (1), 314–331.

Cramer, C. H. (2006) . Quantifying the uncertainty in site amplification modeling and its effects on site-specific seismic hazard estimation in the upper Mississippi embayment and adjacent areas. *Bulletin of the Seismological Society of America* **96** (6), 2,008–2,020.

Cramer, C., J. S. Gomberg, E. S. Schweig, B. A. Waldron, and K. Tucker (2004). *The Memphis, Shelby County, Tennessee, Seismic Hazard Maps*. USGS Open File Report 2004-1294, Memphis, TN, 46 pp.

Eggert, D. L., A. C. Samuelson, J. D. Bray, C. W. Chang, W. R. Eckhoff, K. Kayabali, E. J. McClees, T. R. West, M. C. Woodfield, and B. Zheng (1994). *Final Report to the City of Evansville: Shear-wave and Earthquake Hazard Mapping of Evansville, Indiana*. Open File Studies, OFS94-19, Bloomington: Indiana Geological Survey, 17 pp.

Frankel, A., C. Mueller, T. Barnhard, D. Perkins, E. V. Leyendecker, N. Dickman, S. Hanson, and M. Hopper (1996). *National Seismic Hazard Maps: Documentation June 1996*. USGS Open File Report 96-532, 110 pp.

Frankel, A., M. Petersen, C. Mueller, K. Haller, R. Wheeler, E. V. Leyendecker, R. Wesson, S. Harmsen, C. Cramer, D. Perkins, and K. Rukstales (2002). *Documentation for the 2002 Update of the National Seismic Hazard Maps*. USGS Open File Report 02-420, 33 pp.

Gray, H. H. (1989). Quaternary Geologic Map of Indiana. Indiana Geological Survey Miscellaneous Map 49, 1:500,000, Bloomington, IN.

Green, R. A., S. F. Obermeier, and S. M. Olson (2005). Engineering geologic and geotechnical analysis of paleoseismic shaking using liquefaction effects: Field examples. *Engineering Geology* **76**, 263–293.

Haase, J. S., R. L. Nowack, and Y. S. Choi (2011). Liquefaction hazard near the Ohio River from Midwestern Scenario Earthquakes. *Environmental & Engineering Geoscience,* in press.

Haase, J. S., R. L. Nowack, Y. S. Choi, and T. Bowling (2011). Probabilistic seismic hazard assessment including site effects for Evansville, Indiana, and the surrounding region. *Bulletin of the Seismological Society of America* in press.

Harmsen, S., D. Perkins, and A. Frankel (1999). Deaggregation of probabilistic ground motions in the central and eastern United States. *Bulletin of the Seismological Society of America* **89** (1), 1–13.

Holzer, T. L. (2003). Earthquake Hazards: USGS Cone Penetration Testing Data: Evansville Indiana Area; http://quake.wr.usgs.gov/prepare/cpt/. United States Geological Survey.

Hough, S. E., J. G. Armbruster, L. Seeber, and J. F. Hough (2000). On the Modified Mercalli Intensities and magnitudes of the 1811–1812 New Madrid earthquakes. *Journal of Geophysical Research—Solid Earth* **105** (B10), 23,839–23,864.

Idriss, I. M., andJ. I. Sun (1992). *User's Manual for SHAKE91*. Center for Geotechnical Modeling, Dept. of Civil and Environmental Engineering, University of California, Davis, CA.

Johnston, A. C. (1996). Seismic moment assessment of earthquakes in stable continental regions: II. New Madrid 1811–1812, Charleston 1886 and Lisbon 1755. *Geophysical Journal International* **126** (2), 314–344.

McNulty, W. E., and S. F. Obermeier (1999). Liquefaction evidence for at least two strong Holocene paleo-earthquakes in central and southwestern Illinois, USA. *Environmental and Engineering Geoscience* **5** (2), 133–146.

Moore, D. W., S. C. Lundstrom, R. C. Counts, S. L. Martin, W. M. Andrews Jr., W. L. Newell, M. L. Murphy, M. F. Thompson, E. M. Taylor, E. P. Kvale, and T. R. Brandt (2009). Surficial Geologic Map of the Evansville, Indiana and Henderson, Kentucky Area, 1:50,000 scale. USGS Scientific Investigations Map SIM-3069, Denver, CO.

Munson, P. J., and C. A. Munson (1996). *Paleoliquefaction Evidence for Recurrent Strong Earthquakes since 20,000 yr BP in the Wabash Valley Area of Indiana*. Final technical report for USGS Grant #14-08-0001-G2117, Indiana University, Bloomington, 137 pp.

Munson, P. J., C. A. Munson, and E. C. Pond (1995). Paleoliquefaction evidence for a strong holocene earthquake in south-central Indiana. *Geology* **23** (4), 325–328.

Nuttli, O. W. (1983). *Catalog of Central United States Earthquakes since 1800 of mb = 3.0*. St. Louis, MO: St. Louis University.

Odum, J. K., W. J. Stephenson, and R. A. Williams (2010). Predicted and observed spectral response from collocated shallow, active and passive-source *Vs* data at five ANSS sites, Illinois and Indiana, USA. *Seismological Research Letters* **81** (6), 955–964.

Olson, S. M., R. A. Green, and S. F. Obermeier (2005). Revised magnitude-bound relation for the Wabash Valley seismic zone of the central United States. *Seismological Research Letters* **76** (6), 756–771.

Petersen, M. D., A. D. Frankel, S. C. Harmsen, C. S. Mueller, K. M. Haller, R. L. Wheeler, R. L. Wesson, Y. H. Zeng, O. S. Boyd, D. M. Perkins, N. Luco, E. Field, C. J. Wills, and K. S. Rukstales (2008). *Documentation for the 2008 Update of the National Seismic Hazard Maps*. USGS Open File Report 2008-1128, 60 pp.

Pond, E. C. (1996). Seismic parameters for the central United States based on paleoliquefaction evidence in the Wabash Valley. PhD diss. , Virginia Polytechnic Institute, Blacksburg, VA.

Rudman, A. J., M. E. Biggs, R. F. Blakely, and J. F. Whaley (1973). Statistical studies of Indiana bedrock velocities: Mapping applications. *Proceedings of the Indiana Academy of Science* **83**, 284–290.

Seeber, L., and J. G. Armbruster (1991). *The NCEER-91 Earthquake Catalog: Improved Intensity-based Magnitudes and Recurrence Relations for U.S. Earthquakes East of New Madrid*. NCEER-91-0021, National Center for Earthquake Engineering Research.

Silva, W., N. Gregor, and R. Darragh (2002). *Development of Regional Hard Rock Attenuation Relations for Central and Eastern North America*; http://www.pacificengineering.org/CEUS/Development%20of%20Regional%20Hard_ABC.pdf. Internal report, Pacific Engineering, El Cerrito, CA, 27 pp.

Sipkin, S. A., W. J. Person, and B. W. Presgrave (2000). Earthquake bulletins and catalogs at the USGS National Earthquake Information Center. *IRIS Newsletter* **2000** (1), 2–4.

Somerville, P. G., N. Collins, N. Abrahamson, R. Graves, and C. Saikia (2001). *Ground Motion Attenuation Relations for the Central and Eastern United States*. Final report for USGS grant no. 99HQGR0098, 38 pp.

Stover, C. W., and J. J. Coffman (1993). *Seismicity of the United States, 1568–1989* (rev.). USGS Professional Paper 1527, 418 pp.

Tavakoli, B., and S. Pezeshk (2005). Empirical-stochastic ground-motion prediction for eastern North America. *Bulletin of the Seismological Society of America* **95** (6), 2,283–2,296.

Toro, G. R., N. A. Abrahamson, and J. F. Schneider (1997). Model of strong ground motions from earthquakes in central and eastern North America: Best estimates and uncertainties. *Seismological Research Letters* **68** (1), 41–57.

Tuttle, M. P., E. S. Schweig, J. Campbell, P. J. Thomas, J. D. Sims, and R. H. Lafferty (2005). Evidence for New Madrid earthquakes in A.D. 300 and 2350 B.C. *Seismological Research Letters* **76** (4), 489–501.

Tuttle, M. P., E. S. Schweig, J. D. Sims, R. H. Lafferty, L. W. Wolf, and M. L. Haynes (2002). The earthquake potential of the New Madrid seismic zone. *Bulletin of the Seismological Society of America* **92** (6), 2,080–2,089.

Wald, D. J., V. Quitoriano, T. H. Heaton, H. Kanamori, C. W. Scrivner, and C. B. Worden (1999). "Trinet ShakeMaps": Rapid generation of instrumental ground motion and intensity maps for earthquakes in Southern California. *Earthquake Spectra* **15**, 537–556.

Wells, D. L., and K. J. Coppersmith (1994). New empirical relationships among magnitude, rupture length, rupture width, rupture area, and surface displacement. *Bulletin of the Seismological Society of America* **84** (4), 974–1,002.

Whaley, J. F., R. F. Blakely, K. K. Like, and C. L. James (2002). Seismic refraction data for Indiana (Point Shapefile). Bloomington: Indiana Geological Survey.

Wheeler, R. L., and C. H. Cramer (2002). Updated seismic hazard in the southern Illinois Basin: Geological and geophysical foundations for use in the 2002 USGS National Seismic Hazard Maps. *Seismological Research Letters* **73** (5), 776–791.

Department of Earth and Atmospheric Sciences
Purdue University
West Lafayette, Indiana 47906 U.S.A.
jhaase@purdue.edu
(J. S. H.)